

Article

# High-Temperature Mechanical Properties of 4.5%Al $\delta$ -TRIP Steel

Dayu Chen, Heng Cui \*  and Rudong Wang

Collaborative Innovation Center of Steel Technology, University of Science and Technology Beijing, Beijing 100083, China; g20179075@xs.ustb.edu.cn (D.C.); rdwang87@126.com (R.W.)

\* Correspondence: cuiheng@ustb.edu.cn; Tel.: +86-1367-123-9796

Received: 28 October 2019; Accepted: 18 November 2019; Published: 25 November 2019



**Featured Application:**  $\delta$ -TRIP steel, a product of ultimate tensile strength (UTS) and total elongation (TE) similar to the third generation of advanced high-strength steels (AHSS), is expected to become the materials of automobile safety parts and structural parts.

**Abstract:** The high-temperature mechanical properties of a 4.5% Al-containing  $\delta$ -transformation-induced plasticity (TRIP) steel were studied by using the Gleeble 3500 thermomechanical simulator. The zero ductility temperature (ZDT) and the zero strength temperature (ZST) were measured, and the brittle zones were divided. The phase transformation zone was determined by differential scanning calorimetry (DSC). The temperature of the phase transformation and the proportion of the phase were calculated by the Thermo-Calc software. The ZDT and the ZST of the 4.5% Al-containing  $\delta$ -TRIP steel are 1355 and 1405 °C, respectively. The first brittle zone and the third brittle zone of the steel are 1300–1350 °C and 800–975 °C, respectively. The reason for the embrittlement of the third brittle zone of the 4.5% Al-containing  $\delta$ -TRIP steel is that the  $\alpha$ -ferrite formed at the austenite grain boundary causes the sample to crack along the grain boundary under stress. The ductility of the 4.5% Al-containing  $\delta$ -TRIP steel decreases first and then increases with the increase of the  $\alpha$ -ferrite. When the proportion of the  $\alpha$ -ferrite reaches 37%, the reduction of area (RA) of the 4.5% Al-containing  $\delta$ -TRIP steel is reduced to 44%. The 4.5% Al-containing  $\delta$ -TRIP steel has good resistance to the high-temperature cracking.

**Keywords:** high-temperature mechanical properties; crack-sensitive zone; brittle zones; phase transformation; equilibrium phase diagram

## 1. Introduction

Transformation-induced plasticity (TRIP) steel refers to ultrahigh-strength steel that is ductility-elevated due to gradual martensitic transformation processes in steel structures. When there is a high content of Al in alloying elements (the Al content is higher than 3%), it is found that, during the solidification process, the  $\delta$ -ferrite does not participate in the reaction and remains in the whole temperature range, so it is named  $\delta$ -TRIP steel. Recently,  $\delta$ -TRIP steel, due to its low density, a product of ultimate tensile strength (UTS) and total elongation (TE) (up to 23 GPa·%) similar to the third generation of advanced high-strength steels (AHSS), and excellent welding properties, is expected to become the materials of automobile safety parts and structural parts [1,2]. Yi et al. [3] found an alloy (its precise composition is Fe–0.4C–0.5Mn–0.2Si–0.5Cr–3.5Al wt %), having a density of  $7.455 \times 10^3$  kg/m<sup>3</sup>, is approximately 5% lighter than that without the aluminum addition, which has a density of  $7.8145 \times 10^3$  kg/m<sup>3</sup>. Abedi et al. [4] found a duplex low-density steel with an exact chemical composition of Fe–17.5Mn–8.3Al–0.74C–0.14Si (wt %), having a density of  $6.8 \times 10^3$  kg/m<sup>3</sup>. The measurement shows that the density of a 4.5% Al-containing  $\delta$ -TRIP steel is  $6.8325 \times 10^3$  kg/m<sup>3</sup>, which is

approximately 8% lighter than that with a 3.5 wt % aluminium addition. It is approximately 12.6% lighter than that without the aluminum addition, which has a density of  $7.8145 \times 10^3 \text{ kg/m}^3$ . Many studies have been reported on mechanical deformation properties [5,6], microstructures [7,8], and properties of  $\delta$ -TRIP steel [9,10]. However, there is an insufficient understanding of the high-temperature crack sensitivity of the  $\delta$ -TRIP steel. The influence of high Al content on it is still lacking, so it is necessary to understand its high-temperature mechanical properties further.

There are many researches, which are regarding high-temperature mechanical properties of Nb-containing TRIP steel [11], P-containing TRIP steel [12], twinning-induced plasticity (TWIP) steel [13–15], dual-phase (DP) steel [16], and FeCrAl [17,18]. A Gleeble thermal-mechanical testing machine is a common method for studying high-temperature mechanical properties [19]. He et al. [18] studied the hot ductility of FeCrAl alloys by using a Gleeble thermal-mechanical testing machine and thought the hot ductility of the alloys mostly depends on the temperature rather than the content of Al. The ferritic grain coarsening and the precipitation of carbides result in decreased ductility between 800 and 900 °C. He et al. [18] found high-Cr-content ferrite stainless steel suffers from embrittlement when subjected to temperatures up to around 475 °C, due to the separation of the  $\alpha$  (Fe-rich) ferrite and the  $\alpha'$  (Cr-rich) ferrite and the transformation of the Fe-rich  $\alpha$  phase and the Cr-rich  $\alpha'$  phase to the  $\alpha$ -(Fe,Cr) ferrite phase by using differential scanning calorimetry (DSC). Hechu et al. [20] found the solid-state transformation of a  $\delta$  dendrite core to a single  $\gamma$  phase without a peritectic reaction at 1358 °C. Some researches [15,21,22] show that the increase of Al content leads to a worse hot ductility and high Al content in steel can easily lead to deterioration of surface quality of continuous casting slabs [23]. However, Su et al. [12] found that the increase of Al content in TRIP steel (0.03–0.87% Al) led to an overall increase of a reduction of area (RA) and better hot ductility. It was indicated that the effect of high Al content on the high-temperature mechanical properties of steel is a complicated change. There are many research results on mechanical properties of  $\delta$ -TRIP steel, but research on high-temperature mechanical properties of high-aluminum  $\delta$ -TRIP steel is relatively limited.

In this paper, a high-temperature tensile test was carried out on the Gleeble 3500 thermomechanical simulator, and the characteristic curves were obtained. Brittle zones and a crack-sensitive zone of  $\delta$ -TRIP steel were calculated by the characteristic curves. The fracture morphology of the specimen after the high-temperature tensile fracture was observed by scanning electron microscopy (SEM) to determine the fracture type. The equilibrium phase diagram of the 4.5% Al-containing  $\delta$ -TRIP steel was calculated by the Thermo-Calc software. The phase transformation temperatures of the 4.5% Al-containing  $\delta$ -TRIP steel were measured by the DSC.

## 2. Materials and Methods

A  $\delta$ -TRIP steel ingot was prepared by vacuum induction melting using commercial-purity materials with a target composition of 0.4C–0.5Si–2.0Mn–4.5%Al–Fe (wt %). The dimensions and the shape of the  $\delta$ -TRIP steel ingot are shown in Figure 1. The concentrations of C and S were measured using the infrared absorptiometric method after combustion in current oxygen. Besides, the inert-gas carrier melting–thermoconductometric method was employed for the measurement of N concentration. The contents of the other alloying elements (Si, Mn, and Al) were measured by the inductively coupled plasma optical emission spectrometric (ICP-OES) methodology.

Figure 1 shows the dimensions and the shape of the  $\delta$ -TRIP steel ingot as well as the dimensions and the locations of the specimens. The shape of  $\delta$ -TRIP steel ingot, like an inverted cone, had an upper diameter ( $\Phi$ ) of 120 mm and a total length of 240 mm. Gleeble tensile specimens were cut from the columnar grain region of the ingots. The Gleeble tensile specimens were standard cylindrical tensile specimens, of which the diameter was 10 mm and the length was 121.5 mm. The sampling position of the DSC specimen was near the sampling position of the Gleeble tensile specimens. The DSC specimen was required to have be a round flake with a diameter of 5 mm or a rectangular flake with a diagonal length no more than 5 mm, and its thickness was generally less than 1 mm. Due to the large contents of Al and Mn in the specimen, to minimize the contamination of the instrument support during the

melting process, the DSC specimen size (diameter  $\times$  thickness) in this test was 3 mm  $\times$  1 mm. Drill 6 equidistant holes were in the axis of the  $\delta$ -TRIP steel ingot and had a small amount of steel scrap. A cylindrical specimen with a diameter of 33 mm and a height of 10 mm at the bottom of the ingot was used, and this cylindrical specimen and the steel scrap were analyzed to determine the chemical composition of the ingot.

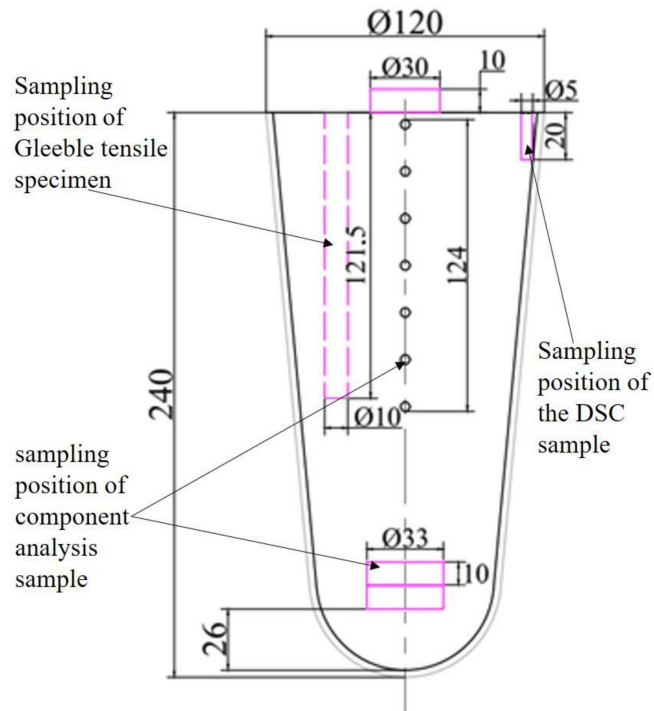


**Figure 1.** Sampling positions and dimensions of the  $\delta$ -transformation-induced plasticity (TRIP) steel ingot and the specimens.

The high-temperature mechanical properties of  $\delta$ -TRIP steel were studied by using the Gleeble 3500 thermomechanical simulator. With the electrical discharge machining (EDM) method to shape the ingot-carved cylindrical tensile steel and the area of the columnar crystal being placed at a temperature range of 700 to 1350 °C, the specimen was tensioned at a constant temperature and at a constant strain rate of  $1 \times 10^{-3} \text{ s}^{-1}$ . All the tests were carried out in an atmosphere of argon to avoid steel oxidation. The temperature control diagram of the tensile test is shown in Figure 2. The steel samples were first heated to 1300 °C with a heating rate of 10 °C/s, and then they were subjected to insulation during the solid solution treatment for 180 s to homogenize the microstructure and eliminate the internal stresses. The steel was cooled at a rate of 3 °C/s for 3 min until its temperature reached the test temperature, which was maintained. At temperatures above 1300 °C, the steel was heated to the test temperature at a rate of 3 °C/s and incubated for another 3 min. Finally, the sample was tensioned until it fractured and cooled rapidly in argon. The measured area reduction was used as a function of the deformation temperature to evaluate the hot ductility behavior. The morphology of the fracture was observed under SEM. The fracture type was analyzed. The RA and the  $\sigma_{\max}$  of the steel were obtained in the high-temperature tensile test. The temperatures, at which both the RA and the  $\sigma_{\max}$  value of the sample were zero, were measured corresponding to the zero ductility temperature (ZDT) and the zero strength temperature (ZST), respectively [24,25].

The solidification path with the equilibrium phase of the  $\delta$ -TRIP steel was studied according to the phase equilibrium fraction diagram, which was calculated by using the Thermo-Calc software and the TCFE9 database.

The rough DSC specimens were finely ground for a smooth surface and a uniform thickness. The phase transformation of the high-aluminium-content  $\delta$ -TRIP steel in a range of 40–1400 °C was

analyzed by DSC. The measurement error of the instrument was within 2.5%, the temperature error was  $\pm 1.5$  °C, and the temperature rise was rated at 10 °C/min during the test. The test was carried out in an inert gas (Ar) using a corundum crucible at a temperature range from 40 to 1400 °C.

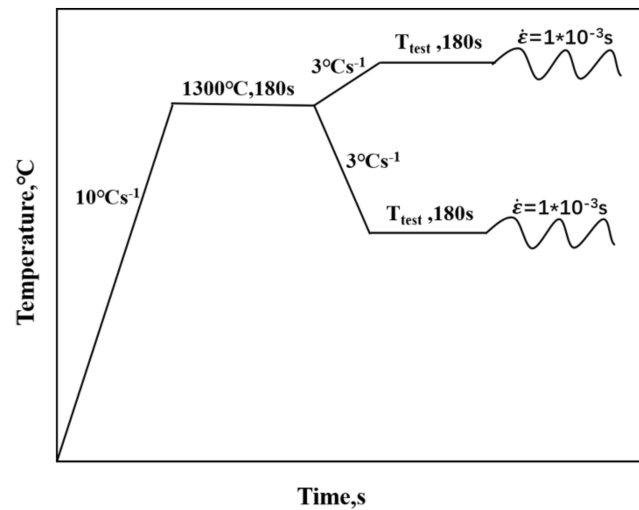


Figure 2. Thermal schedule for the hot tensile tests.

### 3. Results and Discussion

#### 3.1. Hot Ductility

Figure 3 shows the measured tensile strength relative to the temperature.  $\sigma_{\max}$  was decreased with the increasing temperature. Between 700 and 950 °C,  $\sigma_{\max}$  decreased with temperature, while the decreasing speed of the  $\sigma_{\max}$  at the temperatures above 950 °C was significantly slower. The  $\sigma_{\max}$  value was the smallest at 1350 °C, and its value was 1.54 MPa. The measured tensile strength curve was extended by the slope of the final two data points. The ZST of the sample was around 1405 °C.

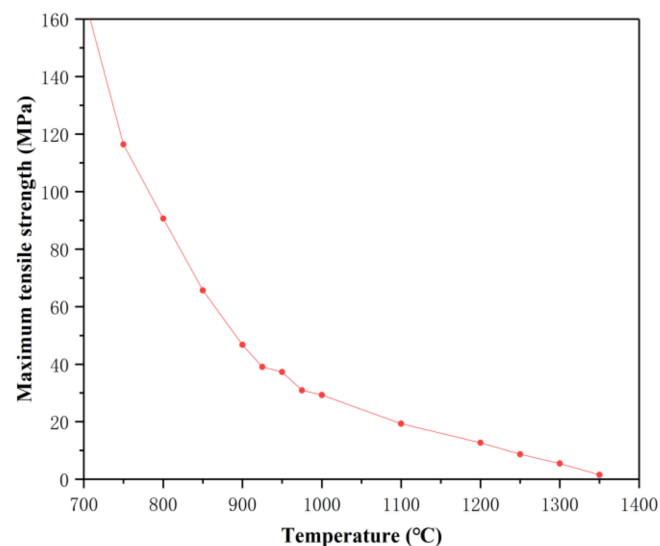
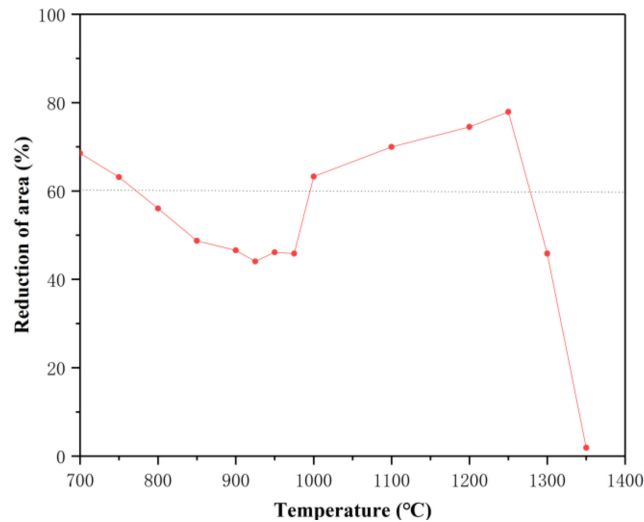


Figure 3. Maximum tensile strength as a function of temperature.

The trend of the RA of the specimen as a function of temperature is shown in Figure 4. In order to better determine the RA of the third brittle zone, the test temperature interval was changed from 50 to 25 °C, and several specimens tested at small temperature intervals were added in the first brittle zone. At a temperature range between 700 and 1300 °C, the RA was basically higher than 40%. In this

temperature range, the minimum value of RA reached approximately 44% at 925 °C. The RA reached its maximum value of 78% at 1250 °C. The RA dropped rapidly between 1250 and 1350 °C. The RA was the smallest at 1350 °C, and its value was 2%. It was indicated that the sample had good resistance to the high-temperature cracking. The RA–temperature curve can be extrapolated. The ZDT of the sample was around 1355 °C.



**Figure 4.** Reduction of area of the specimen as a function of temperature.

$\Delta T$  is the difference between the ZST and the ZDT, which is the temperature range of the crack-sensitive zone. Suzuki et al. [26] thought the embrittlement in zone I of a titanium alloy is related to the solidification cracking and the sensitivity of the solidification cracking may be negligibly small if  $\Delta T$  is less than 50 °C. Li et al. [27] found the  $\Delta T$  of TWIP steel with 0.05% C, 25% Mn, 3% Al, and 3% Si is about 50 °C, which is wider compared with those of other steels. The result also indicates that this TWIP steel has stronger high-temperature crack sensitivity. In this research, the  $\Delta T$  of the sample was 50 °C. The high-temperature crack sensitivity of the 4.5% Al-containing  $\delta$ -TRIP steel is excellent.

The research of Suzuki et al. [28] shows the steel is not easy to crack for  $RA > 60\%$  and the sensitivity of the crack increases for  $RA < 60\%$ . Based on the RA of 60% as a critical value for dividing ductility, we found that the sample had three temperature zones: the first brittle zone (1300–1350 °C), the second ductility zone (1000–1250 °C), and the third brittle zone (800–975 °C).

### 3.2. Fracture Morphology

Figure 5 shows the typical tensile fracture morphologies of the steel at four temperatures (700 °C, 925 °C, 1250 °C, and 1300 °C) under SEM, which corresponds to the tensile fracture morphologies of the typical points in the four regions bounded by an RA of 60, respectively.

Figure 5c shows the tensile fracture morphology of the steel at 1250 °C. It can be seen that the fracture has visible dimple characteristics and the ductility is great. Figure 5c corresponds to the fracture morphology of the highest RA points in the hot ductility curve of the steel.

Due to the microscopic holes generated by the plastic deformation of the steel in the microregion, the nucleation, the growth, and the aggregation were finally connected to each other to cause a fracture, and the diameter and the depth of the dimple were large. The larger the size of the dimples, the better the ductility of the material was. However, the steel with poor ductility had a little change in diameter, the size of the dimple was small and shallow, the shape of the section was flat, the fracture was characterized by the brittle fracture, and the RA was small. Figure 5b shows the fracture morphology of the lowest RA points in the hot ductility curve at 700–1300 °C. The RA was 44% at 925 °C, the dimple had a smaller diameter and a shallow depth, the cross-section was relatively flat, and “rock sugar” particles appeared. The fracture had brittle fracture characteristics, belonging to the

brittle intergranular fracture. Take Figure 5c for example. The crack propagation process before the temperature reached 1250 °C was slow, and it consumed high plastic deformation energy. Therefore, the diameter and the depth of the fracture dimple were large, and there was no flat plane. The fracture was a ductile fracture. At this time, the RA was as high as 78%.

Figure 5d shows the fracture morphology of the steel at 1300 °C. At this time, since the temperature was high, the fracture was composed of a plurality of facets, and the grain boundary was in a molten state.

By comparing the SEM observations, the rock-sugar-shape fracture temperature was found to be above 1300 °C or between 800 and 975 °C. The results are consistent with those of the brittle zones, and the temperature of the dimple fracture was mostly in the range of 1000–1250 °C or 700–800 °C. The observation result is basically consistent with that of the second ductility zone.

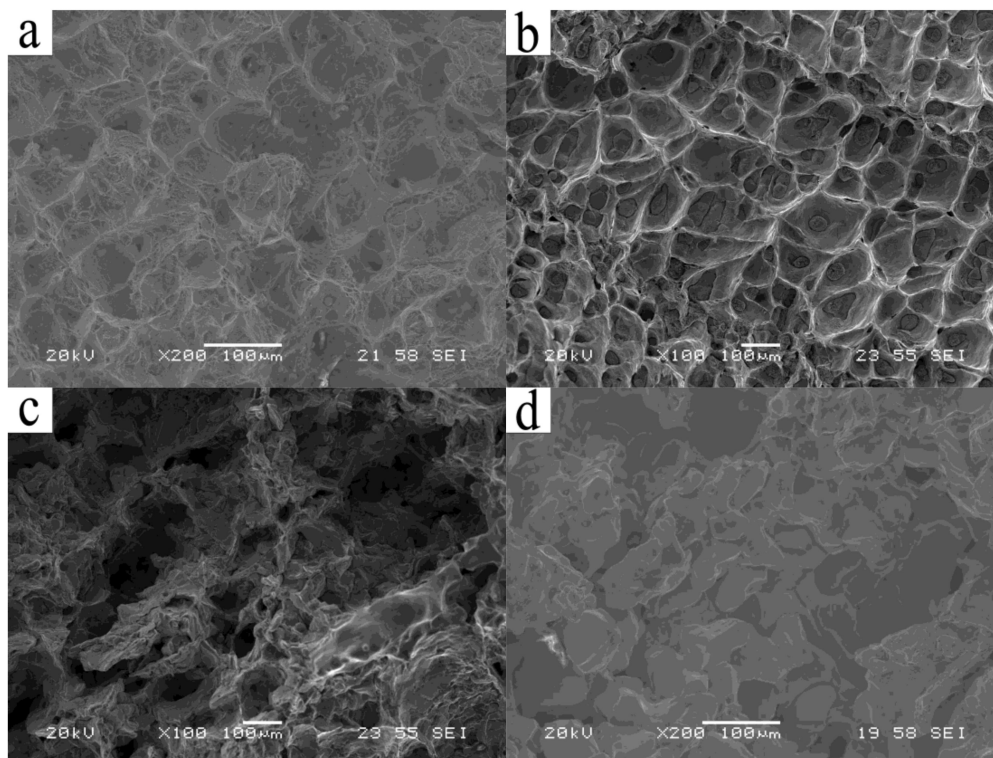


**Figure 5.** Steel tensile fracture morphologies at different temperatures: (a) 700 °C; (b) 925 °C; (c) 1250 °C; (d) 1300 °C.

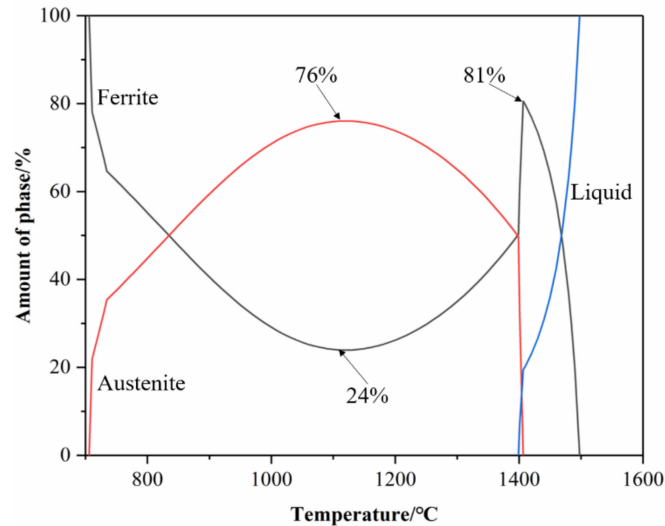
### 3.3. Brittleness Analysis

Figure 6 is a comparison diagram of the high-temperature phase transformation of the sample calculated by the Thermo-Calc software and the TCFE9 database. In Figure 6, the sample did not go through the single-phase ( $\gamma$ ) region, but through ( $\delta + \gamma$ ) two-phase region, in the temperature range of 705–1406 °C. However, the ductility of the sample was excellent due to the fact that most of the RAs were higher than 40%. This is because the amount of the  $\delta$ -ferrite of the sample was high and the proportion of the film-like  $\alpha$ -ferrite was small.

Figure 6 shows that, at the temperatures between 705 and 1406 °C, the  $\delta$ -ferrite was continuously transformed into the  $\gamma$  phase. The proportion of  $\gamma$  increased to 76% at 1100 °C and then began to decrease, and the ferrite content began to rise from 24%. It is speculated that the transformation of the  $\gamma$  phase to the  $\alpha$ -ferrite occurred at this time.

The austenite transformed into the  $\alpha$ -ferrite at the temperature range between 705 and 1100 °C. This indicated that the reason why the ductility of the sample was relatively poor in the third brittle zone is that the massive transforms from the austenite to the  $\alpha$ -ferrite and the primary film-like ferrite grains generated along the austenite grain boundary produced slips. The ductility of the sample

decreased first and then increased with the increase of the  $\alpha$ -ferrite. In the second ductility zone, the sample was in the two-phase regions of the ferrite phase and the  $\gamma$  phase. The ductility of the sample was excellent in the second ductility zone. Al is an element that inhibited the formation of the austenite grains, so that the austenite grains were small and the ductility was excellent.



**Figure 6.** Amount of phase in the 4.5% Al-containing  $\delta$ -TRIP steel.

In the temperature range of 1110–1406 °C, the  $\delta$ -ferrite transformed into austenite, and the crystal structure was transformed from a body-centered cubic to a face-centered cubic. Moreover, within the temperature range of 705–1100 °C, the austenite transformed into the  $\alpha$ -ferrite, the crystal structure was transformed from a face-centered cubic to a body-centered cubic, and the strength of the face-centered cubic crystal was greater than that of the body-centered cubic crystal. With the transformation going on and the  $\alpha$ -ferrite content increasing, this will lead to lowering the substrate ductility.

#### 3.4. Phase Transformation Comparison

In order to compare the actual phase transformation temperature of the sample during heating with the phase transformation temperature by using the Thermo-Calc calculation, the sample was tested by the DSC. Figure 7 shows the DSC analysis curve of the 4.5% Al-containing  $\delta$ -TRIP steel heated from 40 to 1400 °C at a heating rate of 10 °C/min to identify the phase transformation temperature.

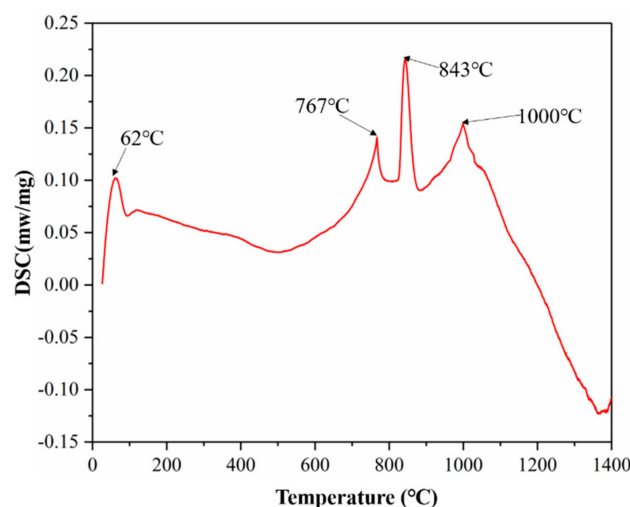


**Figure 7.** Differential scanning calorimetry (DSC) analysis curve.

It can be seen from the figure that there is a significant endothermic peak of the sample at 767, 843, and 1000 °C. It indicates that the matrix transformed from the  $\gamma$  phase to the  $\alpha$ -ferrite at 1000 °C and the phase transformation ended at 767 °C. Ignoring the test error and the instrument temperature fluctuation, the third brittle zone of the sample is consistent with its phase transformation zone. It shows that the reason for the embrittlement of sample in the third brittle zone is the transformation of the austenite to the  $\alpha$ -ferrite. The primary film-like  $\alpha$ -ferrite has low strength and will lead to lowering substrate ductility. The peak temperature of 62 °C is the result of heat-up.

#### 4. Conclusions

1. The ZDT of the sample was 1355 °C, and the ZST was 1405 °C. The  $\Delta T$  of the sample was small. The 4.5% Al-containing  $\delta$ -TRIP steel had good resistance to the high-temperature cracking.
2. The sample had the first brittle zone at 1300–1350 °C and the third brittle zone at 800–975 °C at a constant strain rate of  $1 \times 10^{-3} \text{ s}^{-1}$ . During the continuous casting process, the surface temperature of the slab should be kept away from 800 to 975 °C to reduce the possibility of surface cracking on the slab.
3. The reason for the embrittlement of the third brittle zone of the 4.5% Al-containing  $\delta$ -TRIP steel is that the  $\alpha$ -ferrite formed at the austenite grain boundary caused the sample to crack along the grain boundary under stress.
4. The ductility of the 4.5% Al-containing  $\delta$ -TRIP steel decreased first and then increased with the increase of the  $\alpha$ -ferrite. When the proportion of the  $\alpha$ -ferrite reached 37%, the RA of the 4.5% Al-containing  $\delta$ -TRIP steel was reduced to 44%.

**Author Contributions:** Investigation, D.C.; Methodology, D.C. and H.C.; Data curation, D.C.; Writing of original draft preparation, D.C.; Writing of review and editing, D.C., H.C., and R.W.; Supervision, H.C.; Funding acquisition, H.C.

**Funding:** The research was financially supported by the National Natural Science Foundation of China (grant number: U1860106) and the China Scholarship Council (grant number: 201806465050).

**Acknowledgments:** The authors would like to thank C. Bernhard and P. Presoly from Montanuniversität Leoben for providing access to the Thermo-Calc software and the TCFE9 database.

**Conflicts of Interest:** The authors declare no conflicts of interest.

#### References

1. Yi, H.L.; Sun, L.; Xiong, X.C. Challenges in the formability of the next generation of automotive steel sheets. *Mater. Sci. Technol.* **2018**, *34*, 1112–1117. [[CrossRef](#)]
2. Chatterjee, S.; Muruganath, M.; Bhadeshia, H.  $\delta$ -TRIP steel. *Mater. Sci. Technol.* **2007**, *23*, 819–827. [[CrossRef](#)]
3. Yi, H.L.; Chen, P.; Hou, Z.Y.; Hong, N.; Cai, H.L.; Xu, Y.B.; Wu, D.; Wang, G.D. A novel design: Partitioning achieved by quenching and tempering (Q-T & P) in an aluminium-added low-density steel. *Scr. Mater.* **2013**, *68*, 370–374.
4. Abedi, H.R.; Hanzaki, A.Z.; Liu, Z.; Xin, R.; Haghdadi, N.; Hodgson, P.D. Continuous dynamic recrystallization in low density steel. *Mater. Des.* **2017**, *114*, 55–64. [[CrossRef](#)]
5. Shiri, S.G.; Jahromi, S.A.J.; Palizdar, Y.; Belbasi, M. Unexpected Effect of Nb Addition as a Microalloying Element on Mechanical Properties of  $\delta$ -TRIP Steels. *J. Iron Steel Res. Int.* **2016**, *23*, 988–996. [[CrossRef](#)]
6. Jiao, Z.B.; Luan, J.H.; Miller, M.K.; Yu, C.Y.; Liu, C.T. Effects of Mn partitioning on nanoscale precipitation and mechanical properties of ferritic steels strengthened by NiAl nanoparticles. *Acta Mater.* **2015**, *84*, 283–291. [[CrossRef](#)]
7. Choi, Y.J.; Suh, D.W.; Bhadeshia, H. Retention of  $\delta$ -ferrite in aluminium-alloyed TRIP-assisted steels. *Proc. R. Soc. A Math. Phys. Eng. Sci.* **2012**, *468*, 2904–2914. [[CrossRef](#)]
8. Hwang, S.W.; Ji, J.H.; Lee, E.G.; Park, K.-T. Tensile deformation of a duplex Fe-20Mn-9Al-0.6C steel having the reduced specific weight. *Mater. Sci. Eng. A* **2011**, *528*, 5196–5203. [[CrossRef](#)]
9. Kaar, S.; Krizan, D.; Schwabe, J.; Hofmann, H.; Hebesberger, T.; Commenda, C.; Samek, L. Influence of the Al and Mn content on the structure-property relationship in density reduced TRIP-assisted sheet steels. *Mater. Sci. Eng. A* **2018**, *735*, 475–486. [[CrossRef](#)]

10. Xiong, X.C.; Sun, L.; Wang, J.F.; Jin, X.Y.; Wang, L.; Xu, B.Y.; Chen, P.; Wang, G.D.; Yi, H.L. Properties assessment of the first industrial coils of low-density duplex  $\delta$ -TRIP steel. *Mater. Sci. Technol.* **2016**, *32*, 1403–1408. [[CrossRef](#)]
11. Tuling, A.; Banerjee, J.R.; Mintz, B. Influence of peritectic phase transformation on hot ductility of high aluminium TRIP steels containing Nb. *Mater. Sci. Technol.* **2011**, *27*, 1724–1731. [[CrossRef](#)]
12. Su, H.; Gunawardana, W.D.; Tuling, A.; Mintz, B. Influence of Al and P additions on hot ductility of steels. *Mater. Sci. Technol.* **2007**, *23*, 1357–1366. [[CrossRef](#)]
13. Qaban, A.; Mintz, B.; Kang, S.E.; Naher, S. Hot ductility of high Al TWIP steels containing Nb and Nb-V. *Mater. Sci. Technol.* **2017**, *33*, 1645–1656. [[CrossRef](#)]
14. Liu, H.; Liu, J.; Wu, B.; Shen, Y.; He, Y.; Ding, H.; Su, X. Effect of Mn and Al contents on hot ductility of high alloy Fe-xMn-C-yAl austenite TWIP steels. *Mater. Sci. Eng. A* **2017**, *08*, 60–374. [[CrossRef](#)]
15. Kang, S.E.; Tuling, A.; Banerjee, J.R.; Gunawardana, W.D.; Mintz, B. Hot ductility of TWIP steels. *Mater. Sci. Technol.* **2011**, *27*, 95–100. [[CrossRef](#)]
16. Xiong, Z.P.; Kostyryzhev, A.G.; Stanford, N.E.; Pereloma, E.V. Effect of deformation on microstructure and mechanical properties of dual phase steel produced via strip casting simulation. *Mater. Sci. Eng. A* **2016**, *651*, 291–305. [[CrossRef](#)]
17. He, Y.; Liu, J.; Qiu, S.; Deng, Z.; Yang, Y.; McLean, A. Microstructure and high temperature mechanical properties of as-cast FeCrAl alloys. *Mater. Sci. Eng. A* **2018**, *726*, 56–63. [[CrossRef](#)]
18. He, Y.; Liu, J.; Han, Z.; Deng, Z.; Su, X.; Ji, Y. Phase transformation and precipitation during solidification of FeCrAl alloy for automobile exhaust gas purifying systems. *J. Alloy. Compd.* **2017**, *714*, 251–257. [[CrossRef](#)]
19. Grajcar, A.; Kwaśny, W. Microstructural study on retained austenite in advanced high-strength multiphase 3Mn-1.5 Al and 5Mn-1.5 Al steels. *J. Exp. Bot.* **2012**, *54*, 168–177.
20. Hechu, K.; Slater, C.; Santillana, B.; Clark, S.; Sridhar, S. A novel approach for interpreting the solidification behaviour of peritectic steels by combining CSLM and DSC. *Mater. Charact.* **2017**, *133*, 25–32. [[CrossRef](#)]
21. Li, Z.C.; Misra, R.D.K.; Cai, Z.H.; Li, H.X.; Ding, H. Mechanical properties and deformation behavior in hot-rolled 0.2 C-1.5/3Al-8.5 Mn-Fe TRIP steel: The discontinuous TRIP effect. *Mater. Sci. Eng. A* **2016**, *673*, 63–72. [[CrossRef](#)]
22. Li, Z.C.; Ding, H.; Cai, Z.H. Mechanical properties and austenite stability in hot-rolled 0.2C-1.6/3.2Al-6Mn-Fe TRIP steel. *Mater. Sci. Eng. A* **2015**, *639*, 559–566. [[CrossRef](#)]
23. Cui, H.; Zhang, K.; Wang, Z.; Chen, B.; Liu, B.; Qing, J.; Li, Z. Formation of surface depression during continuous casting of high-Al TRIP steel. *Metals* **2019**, *9*, 204. [[CrossRef](#)]
24. Nakagawa, T.; Umeda, T.; Murata, J.; Kamimura, Y.; Niwa, N. Deformation behavior during solidification of steels. *ISIJ Int.* **1995**, *35*, 723–729. [[CrossRef](#)]
25. Yu, C.H.; Suzuki, M.; Shibata, H.; Emi, T. Simulation of crack formation on solidifying steel shell in continuous casting mold. *ISIJ Int.* **1996**, *36*, S159–S162. [[CrossRef](#)]
26. Suzuki, H.G.; Eylon, D. Hot ductility of titanium alloy: A challenge for continuous casting process. *Mater. Sci. Eng. A* **1998**, *243*, 126–133. [[CrossRef](#)]
27. Li, S.Q.; Liu, J.H.; Liu, H.B.; Zhuang, C.L.; Liu, J.; Han, Z.B. Study on high-temperature mechanical properties of low-carbon Fe-Mn-Si-Al TWIP steel. *High Temp. Mater. Process.* **2017**, *36*, 505–513. [[CrossRef](#)]
28. Suzuki, H.G.; Nishimura, S.; Imamura, J.; Nakamura, Y. Hot Ductility in Steels in the Temperature Range between 900 and 600 C. *Trans. Iron Steel Inst. Jpn.* **1981**, *67*, 1180–1189. [[CrossRef](#)]

